Operational Characteristics of Colloid Thrusters

JULIUS PEREL,* ARTHUR Y. YAHIKU,† JOHN F. MAHONEY† AND HOWARD L. DALEY†
Electro-Optical Systems, A Xerox Company, Pasadena, Calif.

AND

ALLAN SHERMAN‡
NASA Goddard Space Flight Center, Greenbelt, Md.

The operational characteristics of colloid thrusters were determined using experimental testing of several annular emitters and an analytical study based on empirical data. The analytical study was initiated following the exploration of the previously unknown linear region of operation at low-mass-flow rates where the current and thrust vary linearly with extraction voltage and mass-flow rate. This analytical description of colloid operation has reduced the extent of performance-mapping data required to characterize the performance of an emitter-propellant combination. Typical performance mapping includes determinations of thrust, specific impulse, emitter current, and charge-to-mass ratio as functions of emitter voltage and mass flow rate. Emitter performance was upgraded by obtaining stable operation with very low extractor drain currents and with no glow discharge. The relationship between performance level with beam divergence and emitter temperature was also examined. The performance indices and operational curves of a thruster designed to satisfy specific performance goals are derived using the analytical techniques. Methods of achieving improved performance are discussed.

Nomenclature

$f(X)$	=	$X^{-1}(1 - e^{-X})$, dimensionless function
I	=	emitter current, μamp
j	=	current density, amp/m^2
$\dot{m}$	=	mass flow rate, μg/sec-kg/sec
P	=	specific perveance, (amp kg/sec v^3)$^{1/2}$
p	=	space charge perveance, amp/m^2 v$^{3/2}$
q/m	=	specific charge (charge-to-mass ratio), coul/kg
$\langle q/m \rangle = \langle C \rangle$	=	mean specific charge, coul/kg
T	=	thrust, μNewton (μlb)
t	=	temperature, °C
V	=	emitter voltage, kv
$\langle v \rangle$	=	mean particle velocity, m/sec
X	=	$k_o\dot{m}/PV$, reduced parameter
η	=	specific charge distribution efficiency
I_{sp}	=	specific impulse, sec
k_o	=	charge particle generation coefficient, (amp sec/kg v)$^{1/2}$

Introduction

COLLOID thrusters have been under development for near Earth missions because of their high efficiency in the specific impulse range of 500–1500 sec and relatively simple operation. Most of the research and development work in the past has concentrated on capillary needle emitters[1,2] with several hundred needles or more required for most station-keeping and attitude control missions.[3] To eliminate the need for such a large number of emitters, several annular emitter designs were experimentally tested, including one designed and independently tested at Goddard Space Flight Center (GSFC).[4]

Presented as Papers 70-1112 and 70-1113 at the AIAA 8th Electric Propulsion Conference, Stanford, Calif., August 31–September 2, 1970; submitted September 25, 1970; revision received April 28, 1971. Work supported by NASA Goddard Space Flight Center under Contract NAS5-21025.

Index Category: Electric and Advanced Space Propulsion.

* Manager of Particle Physics. Member AIAA.

† Physicist.

‡ Aerospace Engineer. Member AIAA.

Colloid thrusters have demonstrated an extremely wide range of thrust (T) and specific impulse (I_{sp}) levels which can be controlled by varying the mass flow rate ($\dot{m}$) of the propellant, acceleration voltage (V), emitter geometry, emitter temperature, and propellant properties. The complexity of the relationships between these control variables and the operational characteristics of the thruster indicated that parametric analysis of the data would be the most fruitful way to investigate colloid thrusters. Emphasis in the present study was placed on the variation of the operational parameters T,I_{sp}, emitter current (I), and mean specific charge $\langle q/m \rangle$ as a function of control variables V,$\dot{m}$, and temperature for given emitter and propellant combinations. The dependence of $\dot{m}$ upon voltage, temperature, and propellant feed pressure was also investigated. A parallel analytical study provided the means to understand and classify the experimental data and is discussed first. Descriptions of the experimental techniques, emitter configurations tested, and the experimental results follow. A theoretical thruster design using the analytical expressions to predict the operating characteristics of an advanced state-of-the-art emitter is also presented.

Analytical Studies

Analytical models that mathematically describe the operation of a colloid emitter have been the goal of many past studies. Some studies started from the properties of propellant liquids and traced the dynamics of the liquid interface when an intense electric field is applied.[5–7] The resulting equations were compared with experimental results with varying degrees of success. Parametric plots have also been used to display performance data.[8] No quantitative predictability has resulted from either of these approaches, primarily because of a lack of the precise data required to determine the dominant charged particle generating process when competing processes are involved, and from a lack of data over a wide range of control variables.

Experimental data obtained in this laboratory indicated that the performance of a colloid emitter at low $\dot{m}$ was signifi-

cantly different from that at high $\dot{m}$ where most past data were obtained. At low $\dot{m}$, performance was characterized by a linear dependence of I with $\dot{m}$ and V. Operation in this linear region results in desirable performance characteristics such as low beam divergence. A thruster can be operated in this region using the emitter current in a simple feedback control system to regulate the mass flow rate.

Exploration of the low $\dot{m}$ region was considered the key to understanding the operation of colloid emitters and provided a basis for a semiempirical model that shows the dependence of thruster performance (in terms of operational parameters) upon the control variables. This dependence has not been obtained on a purely analytical basis because the generated specific charge depends upon a complex interaction at the emitter edge. This interaction is electrohydrodynamic in nature with the fluid/metal interface in the presence of an intense nonuniform electric field resulting in the generation and acceleration of charged liquid droplets having a specific charge distribution.

The mean specific charge in such a beam of charged particles is defined as

$$\langle q/m \rangle \equiv \langle C \rangle = I/\dot{m} \tag{1}$$

The thrust provided by this beam is given by

$$T = \dot{m}\langle v \rangle \tag{2}$$

where $\langle v \rangle$ is the mean velocity of the particles in the beam. From energy considerations ($qV = 1/2mv^2$) this velocity is related to the accelerating voltage by

$$\langle v \rangle = \langle C^{1/2} \rangle (2V)^{1/2} \tag{3}$$

where $\langle C^{1/2} \rangle$ is the mean root specific charge. The relationship between $\langle C \rangle$ and $\langle C^{1/2} \rangle$ in terms of the specific charge distribution efficiency (η) is

$$\eta = \langle C^{1/2} \rangle^2 / \langle C \rangle \tag{4}$$

This efficiency defines the loss of thrust (or power) as a result of the specific charge distribution. In terms of the experimental data the following expression is obtained from Eqs. (1-4)

$$I/T = \langle C \rangle^{1/2} / (2\eta)^{1/2} V^{1/2} \tag{5}$$

The initial experimental results showed a linear response of T and I as functions of $\dot{m}$ in the low $\dot{m}$ region for constant V. But even more significant was the constant slope over a wide range of T,I,V, and $\dot{m}$ which implied that the slope was a suitable index for classifying the operation of an emitter. These data are shown in Fig. 1 where the slope of the curve is defined as

$$I/T \equiv k_o f(X)/(2\eta)^{1/2} \tag{6}$$

where k_o is a constant for a given emitter-propellant combination termed the charged particle generation coefficient, and $f(X)$ is a dimensionless function of $\dot{m}$ and V that describes the change in the slope of I/T that occurs at higher $\dot{m}$ and by definition is equal to one in the linear region.

From Eqs. (5) and (6) we can write

$$\langle C \rangle = k_o^2 f^2(X) V \tag{7}$$

and from Eqs. (1) and (6)

$$I = k_o^2 f^2(X) V \dot{m} \tag{8}$$

Note from Eq. (7) that k_o^2 (the specific charge per unit volt) has the dimensions coul/kg v and can be considered a charged particle generating index. This term depends upon the properties of the propellant and the electric field at the emitter edge which for a given emitter geometry is proportional to the applied voltage.

To determine $f(X)$, the low $\dot{m}$ (emission limited) and high $\dot{m}$ (space-charge limited) regions are first considered separately

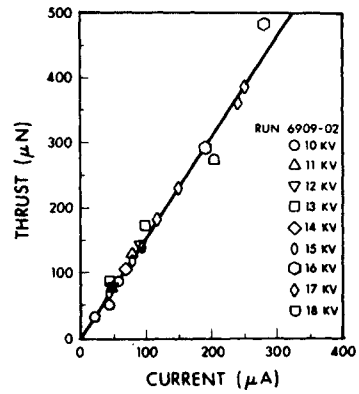

Fig. 1 Thrust vs current for A01, run 6906-02.

since the behavior is significantly different for these two regions. The low $\dot{m}$ region can be characterized by a linear relationship between I and $\dot{m}$ with $f(X)$ equal to unity and therefore Eq. (8) can be reduced to

$$I_l = k_o^2 V \dot{m} \tag{9}$$

At very high $\dot{m}$ the current is assumed to be space charge limited, and can be characterized by the Child-Langmuir equation for current density (j) as given by

$$j = pV^{3/2} \tag{10}$$

where p is the space charge perveance. Since the emission area (A) of an emitter is not well defined and the specific charge varies with the control variables, we introduce the specific perveance $P = pA/\langle C \rangle^{1/2}$, which has the dimensions of (amp kg/sec v^3)$^{1/2}$. Thus Eq. (10) can be written as

$$I_s = \langle C \rangle^{1/2} P V^{3/2} \tag{11}$$

where I_s is the space charge limited current obtained from $I_s = jA$. A smooth transition between the linear and space charge equations can be obtained in Eq. (8) using the following function

$$f(X) = X^{-1}(1 - e^{-X}), \quad \text{if} \quad X = k_o \dot{m}/PV \tag{12),(13}$$

Equation (8) then reduces to Eqs. (9) and (11) at the boundaries $f(X) = 1$ and $f(X) = 1/X$, respectively. The current and other operational parameters such as $\langle C \rangle, T$, and I_{sp} can be determined analytically using the performance indices k_o and P and the control variables $\dot{m}$ and V in the expressions for $f(X)$ and X. The operational parametric equations will not be respecified in a form incorporating Eqs. (12) and (13) so that $\dot{m}$ is implicit in X and $f(X)$. Equation (8) can be rewritten as

$$I = k_o X f^2(X) P V^2 \tag{14}$$

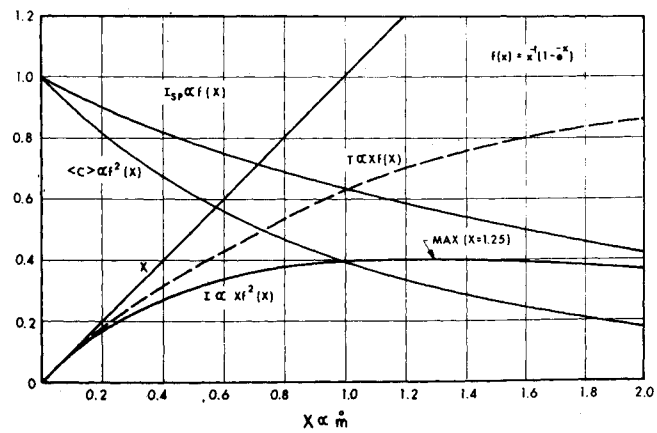

Fig. 2 Variation of operational parameters with $\dot{m}$ at constant k_o, P, V, and η.

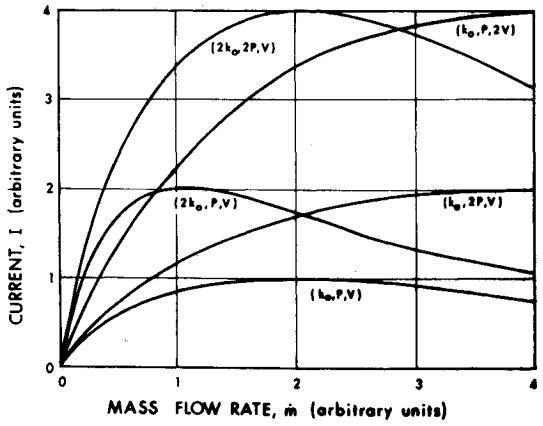

Fig. 3 Current vs $\dot{m}$ for various performance indices and V.

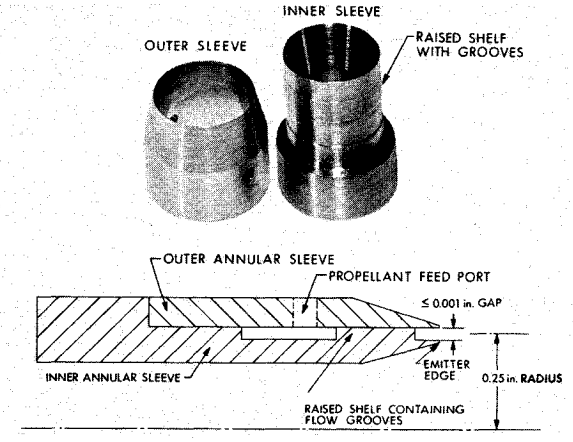

Fig. 5 Photograph and sectional sketch of annular emitter.

where only the term $Xf^2(X)$ is a function of $\dot{m}$. The rest of the operational parameters can be expressed in a similar form

$$T = (2\eta)^{1/2}Xf(X)PV^2 \tag{15}$$

$$I_{sp} = (2\eta)^{1/2}k_o f(X)V/g \tag{16}$$

where g is the acceleration due to gravity on the earth. These equations can be used to display the relationships between the operational parameters and control variables. For this, the indices k_o,P,V, and η are assumed constant so that X is proportional to $\dot{m}$. Equations (7) and (14–16) can then be given in the following forms

$$\langle C\rangle \propto f^2(X), I \propto Xf^2(X) \tag{17),(18}$$

$$T \propto Xf(X), I_{sp} \propto f(X) \tag{19),(20}$$

These relationships are displayed in Fig. 2. Note that $\langle C\rangle$ decreases with $\dot{m}$ (or X) and that I_{sp} decreases less rapidly. The current increases, reaches a maximum, and then decreases, while T continuously increases. The curves display the characteristic variation of the operational parameters as a function of $\dot{m}$. To characterize the operation of a thruster only one of these operational parameters is required as the rest are interrelated as shown in Fig. 2. For the purpose of discussion the current curve was chosen to define the different operating regions as: 1) linear (within 20%), $X \leq 0.2$, $f(X) \approx 1$; 2) transition, $0.2 < X < 2.3$; 3) space charge limited (within 10%), $X \geq 2.3$, $f(X) \approx 1/X = (PV)/(k_o\dot{m})$; 4) position of maximum, $X = 1.25$. Note, for example, that $Xf^2(X)$ is 20% below theoretical linearity at $X = 0.2$ [$f^2(X) = 0.8$] but differs by less than 10% from an averaged straight line $Xf^2(X) \approx 0.9X$. Thus data limited to this linear region and having an experimental error of $\pm 10\%$ can not be distinguished from strict linearity.

To illustrate the effects of varying the performance indices and V, Fig. 3 shows I vs $\dot{m}$ (Eq. 14) in arbitrary units for a thruster with parameters (k_o,P,V). The maximum occurs at $I = 1$, $\dot{m} = 2$, with the linear region slope equal to k_o^2V. If just k_o is doubled, the linear slope increases by a factor of four and the maximum shifts to $I = 2$, $\dot{m} = 1$. If the value of P is doubled, giving parameters (k_o,$2P$,V), the linear slope remains the same as the initial curve, but the maximum shifts to $I = 2$, $\dot{m} = 4$. For parameters ($2k_o$,$2P$,V) the current and linear slope increase by a factor of four. Finally, increasing V by a factor of two increases the (k_o,$2P$,V) curve by a factor of two. Thus, the slope in the linear region can be greatly affected by the value of k_o and somewhat by V as indicated above. The $\dot{m}$ range of the linear region is determined by V and P.

The indices k_o and P characterize the operation of a thruster over the entire usable range of control variables. Thus to compare various emitter-propellant combinations, tests can

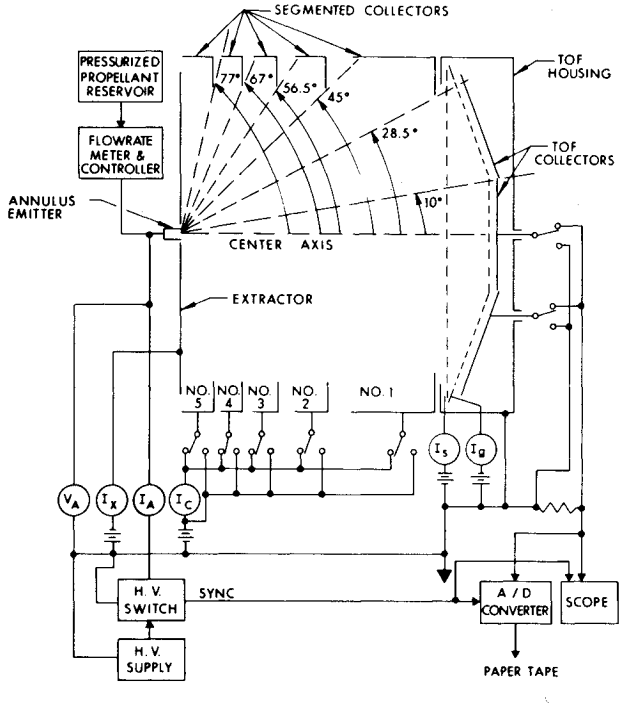

Fig. 4 Schematic diagram of experimental arrangement.

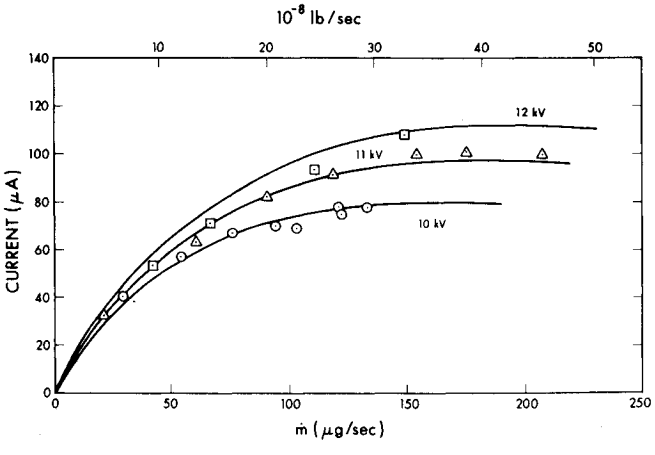

Fig. 6 I vs $\dot{m}$ for A02, run 6910-01.

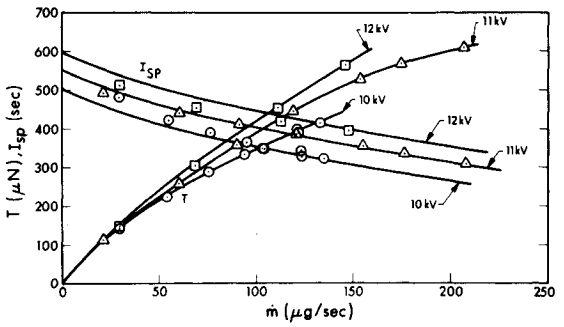

Fig. 7 Thrust and I_{sp} vs $\dot{m}$ for A02 run 6919-01.

be restricted to only those data required to determine the performance indices. Additional data may be required to determine such operational features as emitter temperature effects, general stability, lifetime, etc.

This analysis, together with the experimental studies discussed later, provided information on the physical meaning of the performance indices. The specific perveance (P) appears to be a purely geometric term that, in conjunction with the voltage, determines the accelerating electric field. It depends upon the propellant meniscus shape and the emission area. For example, if an annulus were not emitting from the entire perimeter the value of P would be decreased. This would not affect the value of k_o which depends upon electric field for generating the charged particles in addition to such propellant properties as viscosity, conductivity, surface tension, and perhaps dielectric constant and charge concentration. It was noted that tests involving the dependence of the operational parameters upon the emitter temperature (independent of the mass flow rate) show k_o to be temperature dependent. These tests on temperature effects are discussed later.

Experimental Techniques

A schematic diagram of the experimental arrangement used to obtain emitter data is shown in Fig. 4. The emitters and collectors are located in a 2-ft diam by 3-ft long vacuum chamber having a 10-in. and a 6-in. diffusion pump with liquid nitrogen cooled baffles and cryogenic shroud. These provide pumping speeds which maintain pressures in the 10^{-6} to 10^{-7} torr range during thruster operation.

The collectors consist of a set of segmented cylindrical collectors and a set of two concentric TOF collectors. The TOF collectors have two grids for electrostatic shields with each grid having a transparency of ~98%. The center section subtends a half angle of 10° and an outer section subtends from 10° to 28.5°. Separate coaxially shielded leads for the two sections are brought out of the vacuum chamber so that the TOF collectors can be monitored separately or simultaneously. The current to the TOF collectors is monitored in parallel by an oscilloscope and an analog-to-digital

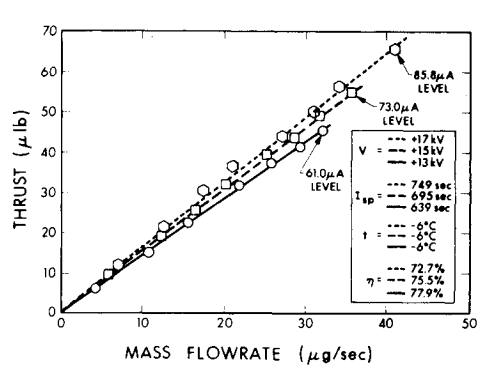

Fig. 8 Thrust vs $\dot{m}$ for A06, run 7004-04.

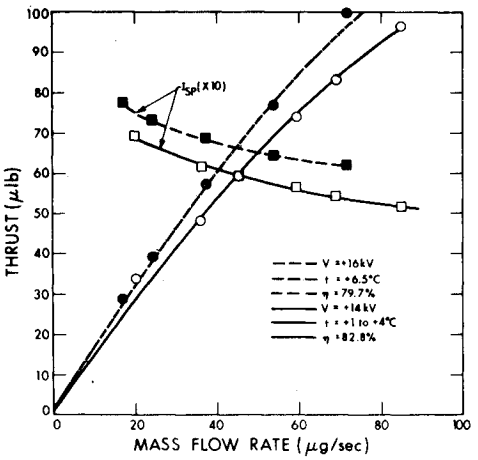

Fig. 9 Thrust and I_{sp} vs $\dot{m}$ for A06 run 7004-02.

data acquisition system (DAS). TOF data are obtained by shorting the high voltage to ground using a switching circuit which provides a sync signal for both the oscilloscope and DAS. The sync signal initiates the TOF trace on the oscilloscope which is recorded with a camera.

The DAS converts the analog current signal to 8-bit binary data points with a resolution of 1% of full scale. The digitizing process occurs at regular time intervals which can be varied from about 2.5 microsec to 0.1 sec. The sync signal from the high-voltage switch initiates the analog-to-digital (A/D) conversion and each digitized data point is stored in a buffer memory having a capacity of 32 data points. When the memory is filled the A/D conversion is stopped. The memory can then be scanned repetitively for display on an oscilloscope by going through a digital-to-analog converter and can also be punched on paper tape. The data from the paper tape are fed into a Sigma 7 computer that is used to calculate the operational parameters and $\dot{m}$, and also provides plots of the operational parameters as a function of $\dot{m}$ for different values of V.

The test propellant (usually 30 g NaI/100 ml glycerol) is fed to the emitter from a pressurized reservoir. Charged particles are generated and accelerated by applying a high voltage (10 kv to 18 kv) to the emitter with the extractors at a negative potential (−1 kv to −4 kv). Thermocouples located $\frac{1}{8}$ in. from the emitter edge were used to monitor the temperature of the emitters.

Emitter Configurations

The basic emitter design in our laboratory consists of two concentric cylinders forming a 0.5-in. diam annulus with an annular gap of 0.001 in. or less. Figure 5 shows a photograph and sectional sketch of the two cylinders of a typical annular emitter containing a raised shelf to restrict the propellant flow

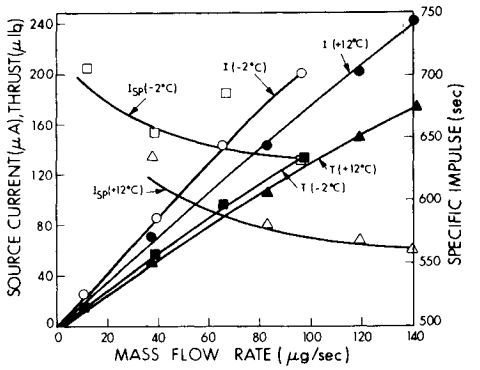

Fig. 10 Thruster performance of A09 at 13 kv.

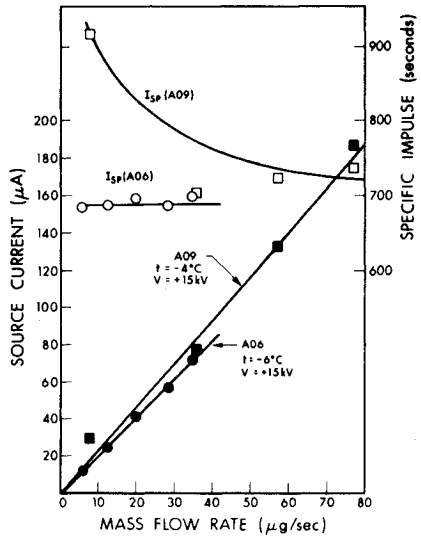

Fig. 11 Thruster performance of A06 and A09 under similar operating conditions.

rate. Extractor electrodes are positioned in the plane of the emitter edge. The GSFC emitter is similarly constructed, but much smaller with an 0.08 in. diameter annulus, a 0.002 in. annular gap, and no inner extractor.

Two emitters are representative of the present state of emitter design. Emitter A06 was designed to have a flat emitter edge and a press-fit annular gap of <0.001 in. To obtain higher specific impulse than that for A06, emitter A09 had a reduced flat at the edge to increase the electric field at a given voltage over that of A06.

Experimental Results

The predicted thruster operational parameters displayed in Fig. 2 were experimentally verified in our laboratory and are also confirmed by the data of other investigators.[6] Data were expressly taken to examine the transition region where the current does not vary greatly with mass flow. Figure 6 displays this region and the linear region for three voltages. The curves drawn through the experimental data points were obtained from the analytical equation (Eq. 14) with the value of k_o obtained from reduced TOF data using Eq. (6). P was determined from the current maximum at $X = 1.25$ (see Fig. 2) using Eq. (13).

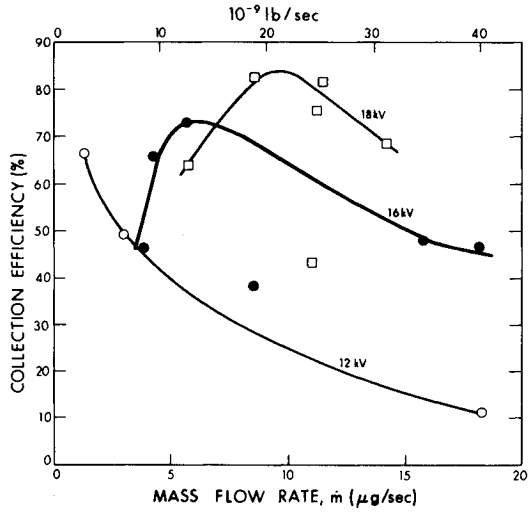

Fig. 12 Collection efficiency vs $\dot{m}$ for emitter GSFC, run 6910-03.

The efficiency (η) was found to change very little for each of the data points so that $(2\eta)^{1/2}$ was considered constant over a run and an average value was used. Figure 7 shows other operational parameter data points and analytical curves for the same run. The agreement between the data points from several runs and the analytical curves was sufficiently good to have confidence in the ability to predict wide-range thruster operation from only a few data points.

Subsequent emitter investigations were designed to optimize performance in the linear region with the effects of the physical properties of operating emitters on the performance indices examined. Emitters edges were then designed to enhance these properties.

Annulus A06 provided a high-mass-flow impedance at the emitter edge which limited operation to the linear region. The thrust-versus-mass flow rate at three different voltages and at constant temperature is shown in Fig. 8. The specific impulse was found to increase with voltage at the rate of 25 sec/kv and changed very little with the mass flow rate. During this test the emitter temperature was maintained constant at −6°C.

Figure 9 shows a plot of thrust versus $\dot{m}$ at higher temperatures for the same annulus (A06). The mass-flow range was extended beyond the linear region by increasing the emitter temperature. The change seen in the operational parameters was primarily due to an increase in voltage, but was offset by the increase in temperature. It should be mentioned that for the data in Figs. 8 and 9 the specific charge efficiency was greater than 70% and remained nearly constant for a given voltage. In general, it has been observed that the specific charge efficiency increases with decreasing voltage.

Operational parameters for annulus A09 are shown plotted in Fig. 10 for two different temperatures. At a constant temperature and voltage, the range of feed pressure and annulus impedance determines the usable mass-flow-rate range. Since annulus A09 has a lower flow impedance than A06, the mass-flow-rate range was extended. The source current and thrust continue to show linearity up to about 120 μg/sec which is the widest range of linearity demonstrated to date. This is an important feature of annulus behavior since this region is most favorable for practical thruster operation and is accompanied by higher specific impulse and better beam focusing. An interesting data point in Fig. 10 is the thrust at 174 μlb achieved at 550 sec by one annulus operated at only 13 kv. The annulus was operated with an electron shield to prevent backstreaming electrons from producing glow discharges and inner extractor currents. The effectiveness of this shield was verified by the low currents (≤1 μamp) when the source was operated up to 250 μamp.

To determine the effect of emitter edge thickness on specific impulse, thruster performance data are plotted in Fig. 11 for A06 and A09 under similar operating conditions. To insure an adequate comparison, data are given at the same voltage (15 kv) for the two annuli. There is a 2°C difference in temperature between these tests. The effect of the smaller edge (A09) clearly results in a higher specific impulse as seen in the figure. In the region between 6 and 40 μg/sec, the specific impulse for A09 lies between 700 and 900 sec while the specific impulse for A06 is in the 690 to 700 sec region.

Beam Focusing Effects

It has been observed in the past that colloid emitters sometimes produce highly divergent charged particle beams. This condition was accompanied by poor performance such as low I_{sp}, etc. Focusing techniques were investigated for capillary needles by shaping or introducing new electrodes.[9] Present measurements of the beam convergence showed a direct correlation between emitter operating region and beam shape. A collection efficiency defined as the ratio of the TOF current to the emitter current was measured for each data run. This

efficiency is a measure of the percentage of the beam confined to a half angle of 28.5° (see Fig. 1).

Figure 12 shows a plot of the collection efficiency versus $\dot{m}$ for the GSFC emitter with curve shapes that clearly illustrate the results from most of the tests. At a constant voltage the efficiency increases with $\dot{m}$ in the linear region. For increasing $\dot{m}$, it reaches a maximum then decreases. The curve shifts to higher values and the maximum to higher $\dot{m}$ as the voltage is increased. Note the poor characteristics at 12 kv where the maximum is below the measured range and the beam is highly divergent at the highest flow rate.

Mass Flow Effects

The effects of various parameters upon mass flow rate were investigated in tests using emitter A06. The results show the mass flow rate to be dependent on voltage, feed pressure, and emitter temperature.

Figure 13 shows a plot of mass flow rate as function of voltage at constant feed pressure. For the voltage range indicated in the plot, $\dot{m}$ varies linearly with the voltage. As a consequence of this variation, the specific impulse remained nearly constant as the source voltage was increased from 10.2 to 17 kv. From a thruster performance standpoint, the specific impulse cannot be increased by increasing voltage if the mass flow varies linearly with voltage. Undoubtedly, this type of variation is not universal and may depend upon the operating level since I_{sp} has been increased by increasing voltage in many of the tests. Nevertheless, this is an important consideration in the design of a thruster system and indicates the importance of a mass flowmeter and controller.

The $\dot{m}$ was found to vary linearly with pressure but with the line having a mass flow intercept at zero pressure (capillary feed). The $\dot{m}$ variation with temperature is directly attributed to the effect of the fluid viscosity which was near exponential in the measured temperature range from −5°C to 20°C.

Temperature Effects

Temperature effects upon the charged particle generation process have been difficult to discern for several reasons. Primarily, it has been masked by the large variation of $\dot{m}$ with temperature, due to the propellant viscosity, and the subsequent variation of specific charge with $\dot{m}$ discussed previously. The temperature, measured at a point on an emitter body, is very close to the value at the emitter edge for an annulus or slit. But the temperature at the tip of a capillary needle can differ by 10–20°C from the measured value due to a large temperature gradient. Temperature control is also difficult in the presence of backstreaming electrons accompanied by large extractor currents and glow discharges.

Using an electron shield to minimize electron backstreaming, extractor current and glow discharge, tests were performed at 15 kv with annulus A06. The data are given in Fig. 14 which shows a plot of the specific charge versus temperature at constant $\dot{m}$. These data also conform to the typical decrease of $\langle q/m \rangle$ with $\dot{m}$, but with some scatter in the data. What is most interesting is the decrease $\langle q/m \rangle$ with increasing temperature at a rate of over 1%/°C. The effect of the decreasing $\langle q/m \rangle$ with increasing temperature at a constant $\dot{m}$ is seen in Figs. 9 and 10.

Summary of Thruster Performance

During the course of this investigation, several other annular emitters were tested and the data analyzed using the equations from the analytical study.[10] The experimental data from the different emitters were reduced to plots of the performance parameters versus the mass flow rate and the results of the test characterized by two performance indices

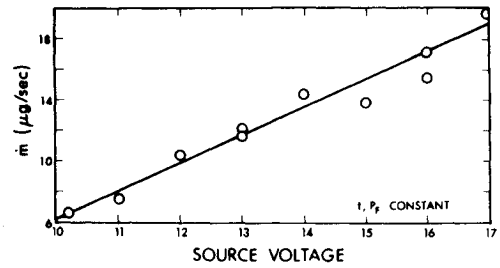

Fig. 13 Variation of $\dot{m}$ with voltage at constant temperature and voltage for A06, run 7002-02.

k_o and P. These indices are dependent upon the propellant properties and emitter geometry where k_o is associated with charge particle generation, and P with particle acceleration. Table 1 contains a listing of the various emitter tests, the propellant mixture batch, and the performance indices. In general, higher values of the performance index result in better performance in terms of achieving high thrust and specific impulse. A given emitter must also be efficient and show stable and controlled operation. For example, A01, in run 6909-02, listed in Table 1, showed very good performance indices, but was unstable and could not be adequately controlled. This was because of lack of temperature control and resulted in poor mass flow control and instability.

The GSFC emitter designed and fabricated at Goddard Space Flight Center[4] had a very low value of k_o. This was probably caused by the lack of an inner extractor. This low value of k_o was also obtained by shorting the inner extractor of A03 to the emitter voltage. This emitter duplicated some of the other performance features of the GSFC emitter including the similar glow patterns. Thus, the value of k_o was in part dependent upon the potential within the annular circle. A06 showed extremely stable operation with good focusing properties which were attributed to the flattened emitter edge. The effect of temperature upon k_o is seen in the results of run 7002-02 in the table. Emitter A09 was an improved design with a smaller flat at the emitter edge in an effort to increase the value of k_o. Tests indicated some improvement with no appreciable loss of focusing properties and stability. The linear region was found to be extended beyond that of other emitters. This is reflected in the large value of P for A09.

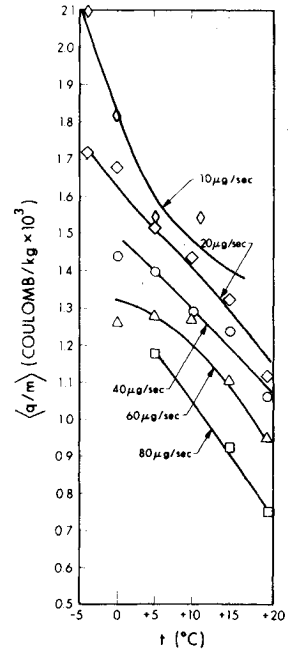

Fig. 14 Variation of specific charge with emitter temperature at several mass flow rates and constant voltage.

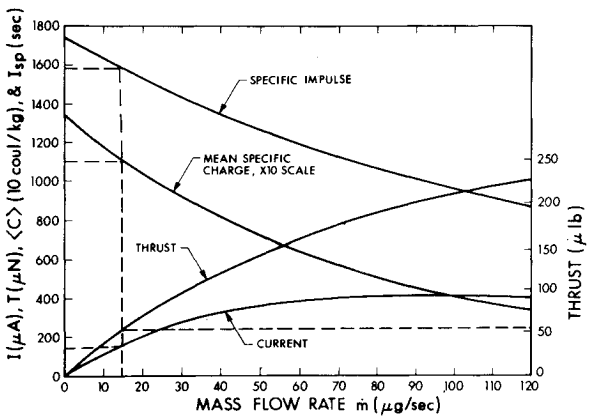

Fig. 15 Operational parameter variation with $\dot{m}$ for a theoretical thruster operated at 15 kv (k_o = 0.95 and P = 47.5 × 10^{-13}).

Theoretical Thruster Design

A thruster can be theoretically designed to satisfy performance goals using the analytical equations. An example is shown to display the use of the analytical curves and the performance indices. The resulting performance curves are particularly useful in understanding the trade-offs that can be made to obtain different operating levels such as the increase in thrust that can be achieved by sacrificing I_{sp}.

For operation of a single emitter at 15 kv and above 1500-sec specific impulse with a specific charge efficiency of η = 72%, a set of performance indices are chosen to be

$$k_o = 0.95 \text{ (amp sec/kgv)}^{1/2}$$

$$P = 47.5 \times 10^{-13} \text{ (amp-kg/sec v}^3\text{)}^{1/2}$$

This combination is near the state-of-the-art for annulus thrusters and will be used for illustrative purposes. With the indices specified, the operational parameters as a function of mass flow rate at constant voltage are shown in Fig. 15. Note that at 53 μlb level where X = 0.2, the current is 165 μamp, $\dot{m}$ is 15 μg/sec and I_{sp} is 1580 sec. The tradeoffs between alternate operational modes are also included in Fig. 15 and are discussed to illustrate the versatility of operation possible with a given thruster. For example, to obtain four times the thrust (200 μlb) at the same voltage, the mass flow can be increased to 93 μg/sec and the current will be 410 μamp, with a resulting specific impulse at ~1000 sec. The operating point is not in the near linear region, but in the constant current region (where I is independent of $\dot{m}$ or where $X > 1$).

An increase in voltage would shift all the curves upward and extend the near linear region out to higher $\dot{m}$. Thus, 250 μlb could be achieved at a higher voltage with a $\dot{m}$ below 100 μg/sec. A thrust of 250 μlb can also be achieved at 900 sec by using two or three annuli having performance indices of $k_o \sim 0.7$ and $P \sim 50 \times 10^{-13}$, and operated at approximately 15 kv and 50 μg/sec each.

Conclusions

The emitter performance discussed here is characterized by stable, repeatable operation with excellent thermal control and good beam focusing properties. The control variables (V,$\dot{m}$, temperature, geometry, and propellants) have been extended over a wide range without encountering glow-discharge or unwanted extractor currents. Using proper shielding techniques, tests have shown that inner extractor currents can be maintained at less than 1% of the total emitter current.

Techniques for data acquisition were introduced which virtually eliminate systematic human error. Data reduction was advanced by the development of an analysis which reduces the operation of an emitter/propellant combination to two performance indices. Since these indices characterize operation over a wide range, they can be used to compare emitter shapes and/or propellants with a greater accuracy than previously achieved. This can also provide a quantitative means for designing emitters and searching for a propellant dopant.

Investigations on temperature effects showed that decreasing the temperature at the emitter edge causes an increase in specific impulse independent of the temperature effect upon mass flow rate.

Beamspread was found to vary with operational level with the maximum focusing at the upper end of the linear region. The region of operation was examined and extended over a wider mass-flow-rate range. In this region the thrust varies linearly with the mass flow rate and voltage, while the specific impulse does not change by more than 10%. Operational level regulation and changes can easily be made using a simple feedback loop.

Table 1 Performance indices of thruster emitters

Emitter	Test	Propellant	k_o amp sec$^{1/2}$ / kgv	P 10^{-13} amp kg$^{1/2}$ / sec v^3	Comments
A01	6908-06	F01	0.48	25	12.5, 13.5 kv
	6909-02	F02	0.79	54	Initial observation of linear operation
A02	6910-01	F02	0.384	51	
GSFC	6910-03	F02	0.266	1.8	12, 14, 16 kv
			0.266	~40	18 kv data only
A03	6912-01	F03	0.43	~57	10, 11, 13 kv
			0.43	~16	9 kv only
			0.252	~50	Inner extractor shorted to emitter
A06	7002-01	F04	0.45	18	Mass flow and temp effects
	7002-02	F05	0.47	12	T = 4°C
					Temp effects
			0.33	11	T = 22°C
	7004-01	F05	0.51	20	Spherical inner extractor (0.25 in.)
	7005-02	F05	0.39	27	Spherical inner extractor (0.31 in.)
A08	7003-01	F04	0.40	6.6	Pt-Ir and SS annulus
A09	7006-01	F05	0.43	200	Extended linear range

References

[1] Perel, J. et al., "Research and Development of a Charge Particle Bipolar Thruster," *AIAA Journal*, Vol. 7, No. 3, March 1969, pp. 507–511.

[2] Huberman, M. N. et al., "Present Status of Colloid Microthruster Technology," *Journal of Spacecraft and Rockets*, Vol. 5, No. 11, Nov. 1968, pp. 1319–1324.

[3] Burson, W. C., "Research on Electrohydrodynamic Charged Droplet Beams," AFAPL-TR-67-199, Oct. 1967, Air Force Systems Command, Wright-Patterson Air Force Base, Ohio.

[4] Stark, K. W. and Sherman, A., "Research and Development in Needle and Slit Colloid Thrusters," TND-5305, Feb. 1970, NASA.

[5] Hendricks, C. D., "Research on High Intensity Charged Particle Sources," AFAPL-TR-67-92, Aug. 1967, Air Force Aero Propulsion Lab., Wright-Patterson Air Force Base, Ohio.

[6] Pfeifer, R. J. and Hendricks, C. D., "Charge to Mass Relationships for Electrohydrodynamically Sprayed Liquid Droplets," *The Physics of Fluids*, Vol. 10, No. 10, Oct. 1967, pp. 2149–2154.

[7] Sherman, A., "Parametric Analysis of Electrostatic Dispersion of a Liquid," X-734-67-321, July 1967, NASA.

[8] Kidd, P. W., "Parametric Studies with a Single Needle Colloid Thruster," *Journal of Spacecraft and Rockets*, Vol. 5, No. 9, Sept. 1968, pp. 1034–1039.

[9] Perel, J., Yahiku, A. Y., and Mahoney, J. F., "Focusing and Deflection of Heavy Charged Particle Beams," AIAA Paper 69-283, March 1969, Williamsburg, Va.

[10] Perel, J., Mahoney, J. F., and Yahiku, A. Y., "Analytical Study of Colloid Annular Thrusters," AIAA Paper 70-1113, Aug.-Sept. 1970, Stanford, Calif.

JULY 1971 J. SPACECRAFT VOL. 8, NO. 7

Pulsed Plasma and Low-Pressure Detonator Thrusters for Secondary Propulsion of Spacecraft

A. V. La Rocca*
General Electric Company-RESD, Philadelphia, Pa.

Recent developments have advanced the pulsed plasma thrusters to the readiness status for long life applications. Lifetimes of several thousands of hours have been repeatedly demonstrated in laboratories and in one flight experiment. A complete system incorporating the latest design techniques is illustrated for application to the stationkeeping and attitude control functions of a 2000-lb 3-axis-stabilized, Earth-synchronous satellite. Current development activities are discussed, including the preliminary study of a dual mode thruster system, which employs the electrically triggered, exothermic fast reactions (detonations) of self-feeding propellant films.

Introduction

SIGNIFICANT progress has been made in the last few years in the development of pulsed plasma accelerators for secondary propulsions. In the SPET Solid Propellant Electrical Thruster Program,[1–6] lifetimes of 10^7 pulses have been repeatedly proven in the laboratory with a system packaged complete with power conditioning and protection logic circuits. Developments in propellant, feed and storage of the so-called inside-out design[4–6] have permitted the passive self-regulating injection of the propellant rate necessary for the thrust in the 0.1–1.0 mlb range for a life of 10^8 pulses eliminating the erosion and hydrodynamic instability problem[7] common to other schemes. A thrust power ratio of 5 μlb/w has been routinely achieved at specific impulses in excess of 1000 sec implying an overall efficiency in excess of 10%. About 25–30% of the losses have been identified to be related to the capacitor and firing loop configuration. Improvement of 10 points in efficiency are expected to be obtainable by proposed modifications of these components. These developments, and others[7–10] have advanced the pulsed plasma microthrusters to the readiness status for long life space applications. Lifetimes of several thousand hours have been repeatedly demonstrated in the laboratories[4–9] and in one flight experiment.[8]

Presented as Paper 70-1147 at the AIAA 8th Electric Propulsion Conference, Stanford, Calif., August 31–September 2, 1970; submitted October 23, 1970; revision received March 9, 1971.

* Consulting Engineer Advanced Propulsion. Associate Fellow AIAA.

Pulsed Plasma Thruster System Application

A multithruster system complete with power conditioning, command and protection logic is presented to illustrate the application of the new design techniques to the stationkeeping and attitude control (A/C) functions of a 3-axis stabilized 2000-lb Earth synchronous satellite. The system consists of 5 multibarrelled completely self-contained thruster subsystems. The hardware consists of combinations of two basic modules: 1) A pulsed plasma thruster module with integrated fuel supply and feed systems, mated to a high energy capacitor of special coaxial design which permits optimum transfer of energy to the thruster barrel. The hollow core of the capacitor accommodates the triggering elements (driving circuit and trigger transformer) of the thruster. 2) A power/command module which can accept the thruster module on one or more of its sides. Up to four thrusters per power/command module are used in this application.

The approach entails designing the modules for the most demanding specs encountered in the foreseeable applications and thus results in modules over-sized (in terms of thrust and power handling capabilities) for the majority of the applications. However this approach results in the following advantages: 1) Reliability is increased by operating at very understressed conditions for many of the long life applications and by having standard modules which can be extensively tested and fully qualified. 2) Interface problems which usually arise from the separation of the power-command module from the thruster modules are eliminated and no high voltage connecting leads are required. 3) The most